Applied Catalysis B: Environmental 238 (2018) 664–671

Contents lists available at ScienceDirect

Applied Catalysis B: Environmental

journal homepage: www.elsevier.com/locate/apcatb

Cobalt-based cubane molecular co-catalysts for photocatalytic water oxidation by polymeric carbon nitrides

Zhishan Luo, Min Zhou, Xinchen Wang*,[1]

State Key Laboratory of Photocatalysis on Energy and Environment, College of Chemistry, Fuzhou University, Fuzhou, 350002, People's Republic of China

ARTICLE INFO

Keywords:
Photocatalysis
Polymeric carbon nitride
Water oxidation
Cobalt cubane
Molecular co-catalyst

ABSTRACT

In artificial photocatalysis, sluggish kinetics of hole transfer and the high recombination rate of charge have been the Achilles' heel of photocatalytic conversion efficiency. The development of co-catalysts for promoting exciton splitting and charge separation has therefore gained continuous attention. Herein, "Co_4O_4" cubane complex $Co_4O_4(O_2CMe)_4(py)_4$ (**1a**, py = pyridine derivatives), serves as a homogeneous molecular co-catalyst which is engineered into the framework of pristine polymeric carbon nitride (PCN) for water oxidation with light illumination. This modification strategy maximizes the contact areas between co-catalysts and reactants, reduces the over-potential of oxygen producing and accelerates the interface transfer rate of electron-hole pairs, thus leading to enhanced reaction kinetics for photocatalytic water oxidation. Compared with pristine PCN, the photocatalytic O_2 production rate up to 19-fold-enhanced in the presence of molecular co-catalyst. This work emphasizes the importance of developing effective, stable and earth-abundant molecular co-catalysts for the promotion of water-splitting photocatalysis.

1. Introduction

The energy sources crisis and environment damage become an obvious challenge in modern science and technology. Water splitting to produce hydrogen and oxygen gases driven by sunlight is an ideal way to address the demand of global energy production, while reducing the negative impact on the environment [1,2]. Nevertheless, the overall efficiency of the oxygen evolution is unsatisfied, ascribing to the high over potential and multi-electron/proton transfers during the complicated 4-electron transfer process. The development of water oxidation catalysts (WOCs) to cooperate with light-energy transducers for high solar energy conversion by water splitting is still a challenge [3]. Therefore, developing efficient and sustainable WOCs that can reduce over-potentials and maximize the extraction of charge carriers while suppressing their recombination is a key measure for photocatalytic water oxidation [4,5].

The polymeric carbon nitride (PCN) seems to be a promising candidate for photocatalytic water oxidation due to its unique electronic band structure, earth-abundant, inexpensive, metal-free and good (photo) chemical stability [6–12]. Although the PCN exhibits excellent hydrogen production [13,14], CO_2 reduction [15–17] and environmental purification [18,19], its ability of water oxidation is particularly limited. To enhance the performance of water oxidation, various chemical modifications, such as doping [20,21], sensitizing [22,23], nanostructure engineering [24–26], copolymerization [27–29] and hybridization [30,31] have been used in the adjustment of PCN framework or even crystalline graphitic carbon nitride materials. Among these various methods, loading PCN with co-catalysts seems to be an efficient, simple and cost-effective strategy, because the co-catalysts not only provide trapping sites for the photogenerated charges, but also promote charge separation kinetic on the surface [32], thus, leading good results of water oxidation [33].

Up to now, noble-metal oxides (such as RuO_2 and IrO_2) are usually used as co-catalysts for hole transport since they can effectively lower the over-potential for the oxidation reaction [34,35]. But subjected to their high toxicity, availability and high costs of upscaling, several low toxicity, earth-abundant and cost-effective co-catalysts (such as CoO_x, Co_3O_4, Co-Pi, MnO_x, NiO_x, Fe_2O_3 and so on) have also been exploited [36–40]. In general, most of these solid co-catalysts are combined with photocatalysts to form solid-state materials for water oxidation. However, these strategies through solid-state co-catalyst loading is potentially limited by finite contact areas between co-catalyst and reactants, and the lack of sufficient active sites for catalysis [41]. In addition, the loading method of co-catalysts not only determines its physical and chemical properties, but also affects the structure of base photocatalytic activity. It is widely accepted that homogeneous catalysis is not

* Corresponding author.
E-mail address: xcwang@fzu.edu.cn (X. Wang).
[1] Http://wanglab.fzu.edu.cn.

https://doi.org/10.1016/j.apcatb.2018.07.056
Received 15 May 2018; Received in revised form 17 July 2018; Accepted 19 July 2018
Available online 27 July 2018
0926-3373/ © 2018 Published by Elsevier B.V.

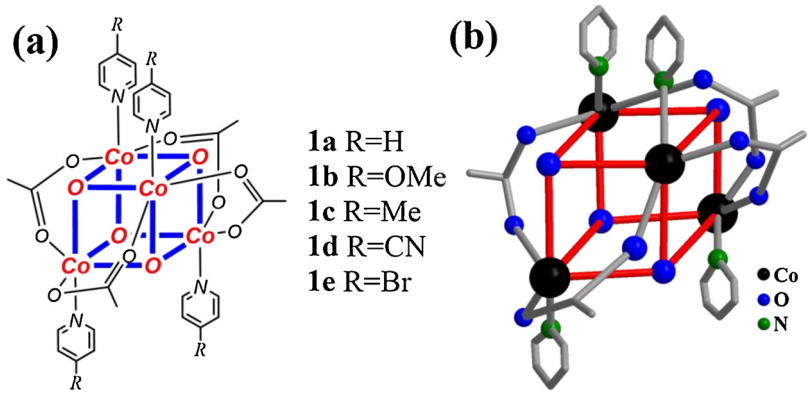

Fig. 1. (a) Molecular structures of the Co_4O_4 cubane catalysts. (b) Ball-and-stick representation of complex **1a**. Carbon and Hydrogen atoms are omitted for clarity.

restricted by the contact area due to its high activity and selectivity [42], which has received considerable attention. For example, hydrogenase and its artificial mimetics for biochemical hydrogen production and newly developed transition metal complexes are considered to be a new type of H_2 evolutionary catalyst [43]. Photosynthetic water oxidation of natural photosynthesis with Mn_4CaO_x clusters of photosynthetic system II also stimulated the development of artificial O_2-evolution catalysts [44,45]. The process in this field focused mainly on molecularly-based systems will provide important opportunities for construction of molecular WOCs [46,47]. It is worth noting that most of these photocatalysts are poor water solubility and low stability, their photocatalytic reaction process must be carried out in organic systems, which is neither economical nor environmentally benign. To this end, the development of water-soluble molecular co-catalysts in the photocatalytic system is essential to achieve cost-effective, earth-abundant and highly efficient man-made photocatalysis.

The $Co_4O_4(O_2CMe)_4(py)_4$ complexes (**1a**, Fig. 1) are especially attractive due to their structural similarity to the oxygen-evolution center of photosystem II in nature [48–51], which is originally reported by Christou and co-works, with a structural cobalt residency in the cube [52]. Over the years, a great deal of research has been conducted on "Co_4O_4" in both experimental and the theoretical aspects [53–56]. Very recently, Wang and co-workers have developed the Co_4O_4 combined with $BiVO_4$ for photocatalytic water oxidation [57], and photoelectrochemical water splitting [58], which has a great efficient. However, large over-potentials are required to drive the oxidation of water under neutral conditions, and the most important is that the Co_4O_4 cannot be directly used as a photocatalyst in water oxidation without any photochemical oxidation sources [48–51], which greatly limits the efficiency of the oxygen evolution reaction. In this work, PCN is operated under basic conditions combined with the molecular Co_4O_4 to reduce the over-potential of oxygen evolution reaction and accelerate the transfer rate of electron-hole pairs (Scheme 1). Electron paramagnetic resonance (EPR) together with photoluminescence (PL) spectra reveal that photogenerated electrons in PCN conduction band readily react with the Ag^+ ions and simultaneously the highly reactive photogenerated holes can easily transfer to the molecular Co_4O_4, eliminating the main competitive pathway of electron-hole recombination. Moreover, evident reduced over-potential can be observed when combined the PCN with molecular Co_4O_4 through the electrochemical test, which is the primary factor behind the improved photocatalytic water oxidation performance. The water-soluble molecular co-catalyst represents a new, simple, and highly effective approach to suppress recombination of photogrenrated charges, which is not affected by the limited contact areas between co-catalysts and reactants, providing sufficient active sites for catalysis and new opportunities for the development of efficient photosynthesis.

2. Experimental

2.1. Materials

All chemicals are of analytical grade and were used as received without further purification. Urea, cobalt(II) nitrate hexahydrate [$Co(NO_3)_2{\cdot}6H_2O$], sodium acetate trihydrate ($CH_3CO_2Na{\cdot}3H_2O$), hydrogen peroxide, 30% (H_2O_2), pyridine (C_5H_5N), dichloromethane (CH_2Cl_2), sodium sulfate anhydrous (Na_2SO_4) and ammonia solution ($NH_3{\cdot}H_2O$) were obtained from Sinopharm Chemical Reagent Co., Ltd. (Shanghai, China). 4-methoxypyridine, 4-methylpyridine, 4-bromopyridine hydrochloride and 4-cyanopyridine, were purchased from Aladdin.

2.2. Synthesis of PCN

PCN was synthesized by annealing urea (10 g) at 550 °C for 2 h under the muffle furnace with the ramping rate at 5 °C/min, and the resulted buff powder was collected.

2.3. Synthesis of $Co_4O_4(O_2CMe)_4(py)_4$, (1a)

Complex **1a** was synthesized according to the literature procedures [53]. Typically, $Co(NO_3)_2{\cdot}6H_2O$ (2.9 g, 10 mmol) and $CH_3CO_2Na{\cdot}3H_2O$ (2.7 g, 20 mmol) are stirred in methanol (30 mL) and heated to refluxing temperature, and pyridine (0.8 mL, 10 mmol) is added to the stirred reaction mixture. A portion of 30% hydrogen peroxide (v/v, 5 mL, 50 mmol) is slowly added to the reaction mixture, and stirring under a refluxing condition is continued for 4 h, then allowed to cool to room temperature. After reducing the volume of the mixture, the latter was introduced to a separating funnel and CH_2Cl_2 was then added. The pink aqueous phase was discarded, while the dark green organic phase dried over anhydrous Na_2SO_4, then filtered. After evaporation of the solvent, a dark green solid was obtained. Yield: 1.5 g (70% based on cobalt). ^1H NMR (500 MHz, D_2O): 8.20(d,8 H), 7.71(t,4 H), 7.20(t,8 H), 2.06 (s, 12 H). FT-IR (KBr, pollet; wavenumber, cm^{-1}): 3417 (w, br), 3110 (w), 3077 (w), 2927 (w), 1608 (m), 1535 (m), 1483 (s), 1452 (s), 1415 (vs), 1342 (w), 1213 (m), 1157 (m), 1074 (m), 1043 (w), 1016 (w), 759 (s), 692 (s), 634 (s), 574 (s) and 453 (w).

$Co_4O_4(O_2CMe)_4(4\text{-}OMepy)_4$, (**1b**); $Co_4O_4(O_2CMe)_4(4\text{-}Mepy)_4$, (**1c**); $Co_4O_4(O_2CMe)_4(4\text{-}CNpy)_4$, (**1d**) and $Co_4O_4(O_2CMe)_4(4\text{-}Brpy)_4$, (**1e**) were also prepared following the reported methods [53]. The main procedure was similar with preparing complex **1a** except using 4-methoxypyridine, 4-methylpyridine, 4-cyanopyridine and 4-bromopyridine hydrochloride to replace pyridine, respectively (Fig. S1).

2.4. Synthesis of CoO_x deposited PCN

0.1 g PCN and a certain amount of $Co(NO_3)_2{\cdot}6H_2O$ were mixed together in 10 mL pure water to form a homogenous solution. Then, it

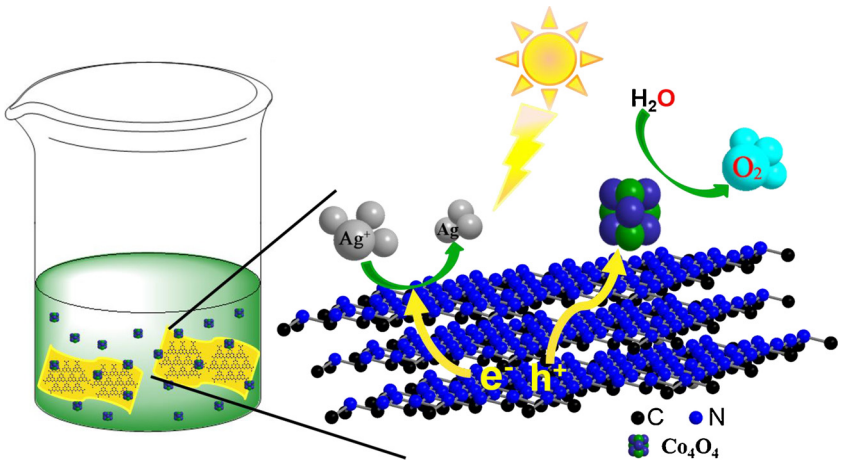

Scheme 1. A schematic representation of photocatalytic oxygen evolution by **1a**/CNU hybrid system.

was evaporated with water vapor to generate a solid mixture. After grinded into powder, they were placed in a crucible with a cover to polymerize the precursors in a muffle furnace at 300 °C for 1 h. The final products were obtained after naturally cooled down to the room temperature.

2.5. Synthesis of $Co(OH)_2$ deposited PCN

0.1 g PCN and a certain amount of $Co(NO_3)_2{\cdot}6H_2O$ were mixed together in 10 mL pure water. After stirring and ultrasonication for 10 min, 1.5 mL $NH_3{\cdot}H_2O$ was added dropwise into the above solution, and a green precipitate was immediately formed. The final resultant sample was obtained after evaporation and drying in an oven at 80 °C for 12 h.

2.6. Impregnation of carbon nitride with Co_4O_4

Co_4O_4 powder was previously dispersed in deionized water with the desired concentration (1.0 mg/mL). Then, PCN powder was dispersed in 5 mL deionized water and sonicated for 10 min. After that, a certain of the Co_4O_4 solution was added to the mixture and stirred for several time. Finally, the mixture is concentrated in a rotary evaporator (Fig. S2). The loading amount was based on the weight of PCN.

2.7. Characterization

Powder X-ray diffraction (XRD) patterns were collected on Bruker D8 Advance diffractometer with Cu-K1 radiation (λ = 1.5406 Å). Fourier transform infrared (FT-IR) spectra were performed on a thermo Nicolet Nexus 670 FTIR spectrometer with KBr as the diluents. Transmission electronic microscopy (TEM) was obtained using a FEI TECNAIG2F20 instrument, the high angle annular dark field (HAADF) images were recorded at 200 keV with a resolution around 1.8 Å. The relatively large collection angle (54–200 mard) of the HAADF detector ensures the excellent atomic-number (Z) sensitivity. [59] X-ray photoelectron spectroscopic (XPS) measurements were performed on an ESCALAB 250 (Thermo scientific, USA) by using a monochromatized Al Kα line source (200 W). The UV–vis reflectance spectra (DRS) were recorded on a Varian Cary 500 Scan UV–vis system. Photoluminescence (PL) spectra were recorded on an Edinburgh FI/FSTCSPC 920 spectrophotometer. Electron paramagnetic resonance (EPR) measurements were carried out on a Bruker model A300 spectrometer. Electrochemical measurements were conducted with a Biologic VSP-300 Electrochemical System in a conventional three electrode cell, using a Pt plate as the counter electrode and a saturated calomel electrode (SCE) as the reference electrode, the active area is confined to 0.25 cm^2.The working electrode was prepared on indium-tin oxide (ITO) glass that was cleaned by sonication in ethanol for 30 min and dried at 353 K. The boundary of ITO glass was protected using Scotch tape. The 5 mg sample was dispersed in 1 mL of DMF by sonication to get a slurry. The slurry was spread onto pretreated ITO glass. After air-drying, the working electrode was further dried at 393 K for 2 h to improve adhesion. Then, the Scotch tape was unstuck, and the uncoated part of the electrode was isolated with epoxy resin. The ^{1}H NMR experiments were performed on a Bruker AVANCE III 500 BBFO 5 mm probe (solution).

2.8. Photocatalytic test for water oxidation

Photocatalytic O_2 production was carried out in a Pyrex top-irradiation reaction vessel connected to a glass closed gas circulation system. For each reaction, 50 mg catalyst powder was well dispersed in an aqueous solution (100 mL) containing $AgNO_3$ (0.01 M) as an electron acceptor and La_2O_3 (0.2 g) as a pH buffer agent. The reaction solution was evacuated several times to remove air completely prior to irradiation with a 300 W Xeon lamp with a working current of 15 A (Shenzhen ShengKang Technology Co., Ltd, China, LX300 F). The wavelength of the incident light was controlled by applying some appropriate long-pass cut-off filters. The temperature of the reaction solution was maintained at room temperature by a flow of cooling water during the reaction. The evolved gases were analyzed *in-situ* by gas chromatography equipped with a thermal conductive detector (TCD) and a 5 Å molecular sieve column, using Argon as the carrier gas.

3. Results and discussion

At the beginning of our study, the simplest Co_4O_4 cubane **1a** was selected to incorporate into the PCN as a molecular co-catalyst. The PCN was synthesized by urea as starting materials, and the thus obtained sample was denoted as CNU. To investigate the local structure of **1a** and **1a**/CNU, power X-ray diffraction (XRD) patterns were utilized to elucidate. XRD patterns of the samples are shown in Fig. 2. We can see four peaks at 10.0°, 10.4°, 11.3° and 14.3° from the Fig. 2a. The most intense XRD peak in Fig. 2b located at 2 θ = 27.4° is a characteristic peak of graphitic stacking, while the other one at 2 θ = 13.0° can be contributed to the structural repeating units of tri-s-triazine [60]. It is interesting that some difference can be viewed in Fig. 2b, with the increasing content of **1a**, the peak at 13.0° and 27.4° are gradually decreased, but the peak at 10.0° and 10.4° are increased. It indicates that **1a** was incorporated in the CNU framework homogeneously not only in the surface, but also between interlayers. Moreover, the reduction of peak at 13.0° is greater than the peak at 27.4°, indicating that the content of **1a** absorbed in the surface of CNU is more than the interlayers. In addition, no evident change except for clearly reduced peak

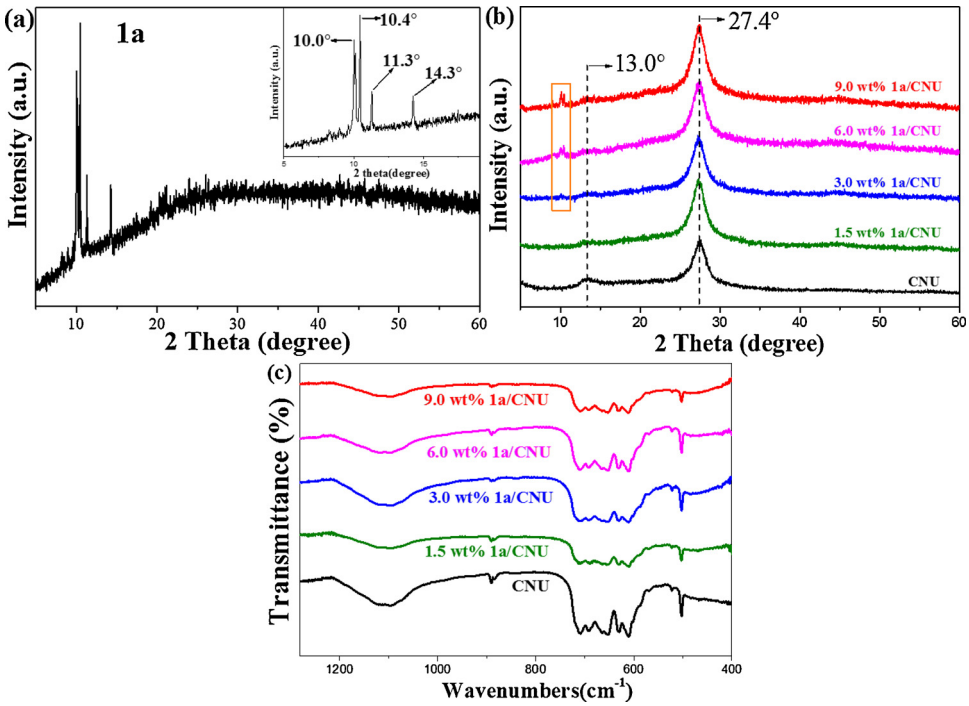

Fig. 2. Power XRD patterns of (a) **1a** and (b) pure and modified CNU samples. (c) FT-IR spectra of CNU and modified with different content of **1a** samples.

intensity of CNU could be seen when the deposited amount increased, indicating the robust properties of the CNU polymer. The FTIR spectra can also prove that the **1a** modified method does not change the structure of CNU (Fig. 2c). The sharp peaks at 805 cm^{-1} is attributed to the breathing mode of the heptazine heterocyclic ring (C_6N_7) units, while the strong bands at 1200–1600 cm^{-1} are related to the stretching variations of the repeating units [23,61].

To give a direct exhibition of the texture, TEM characterization was performed. In Fig. 3a, a similar typical graphitic stacking structure can be checked for modified CNU. This indicates that the basic morphology does not change after modification. To further illustrate the distribution of the catalysts, scanning transmission electron microscopy (STEM) was carried out. In Fig. 3b, it shows the HAADF-STEM image of **1a**/CNU. There is no accumulation of particles on the surface of CNU, which suggests that the elemental mapping characterizations. The elemental mapping pictures of C, N, O and Co elements for the selected area are shown in Fig. 3c-f. This indicates that the **1a** is highly dispersed on the soft carbon nitride framework, enabling the modification of optical/electric and surface properties. In addition, the existence of **1a** can be further certified by high-resolution XPS and EDX analysis (Fig. 4, S3). In Fig. 4a, two weak peaks with binding energy of 780.6 eV and 796.3 eV are ascribed to Co $2p_{3/2}$ and Co $2p_{1/2}$. In Fig. 4b, the binding energy of O 1s is located at 531.7 eV. Two single peak of C 1s locating at 284.6 eV and 288.1 eV in Fig. 4c can be checked. The former one is attributed to

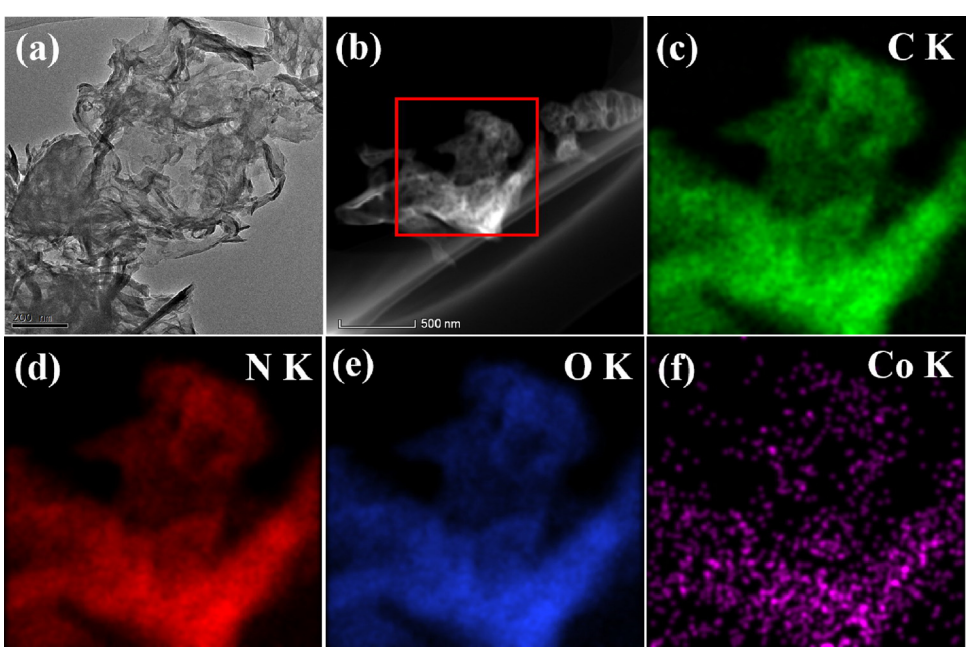

Fig. 3. (a) TEM image, (b) HAADF-STEM image and (c–f) elemental mapping of C, N, O and Co images for **1a**/CNU sample.

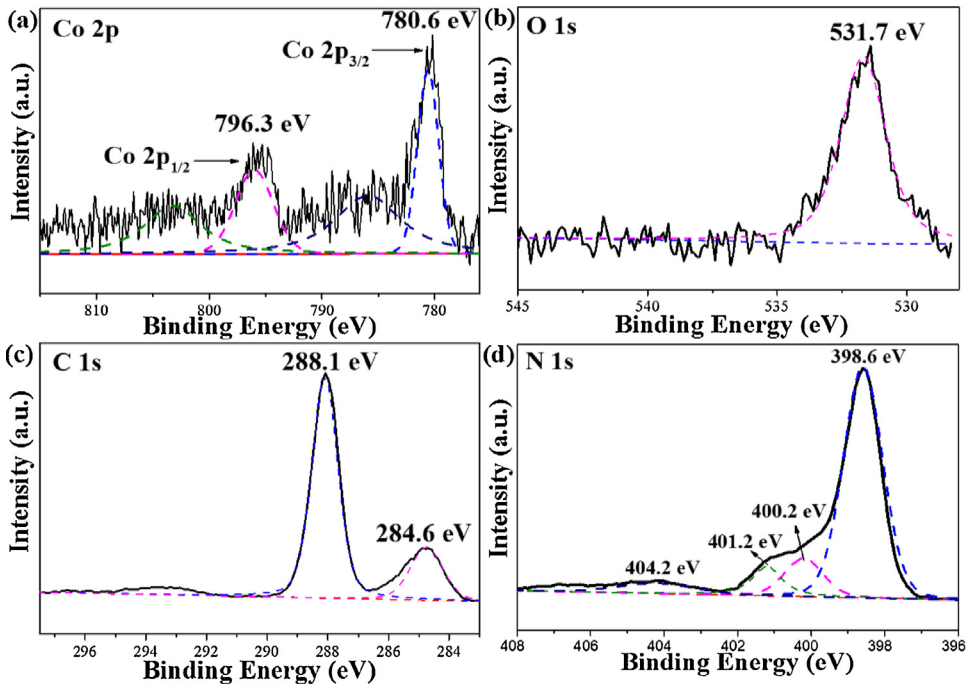

Fig. 4. High resolution XPS spectra of (a) Co 2p, (b) O 1s, (c) C 1s and (d) N 1s for **1a** modified CNU sample.

the sp^2 hybridized C—C bonds, which is determined as the standard carbon. The later one is related to the sp^2-bonded carbon in the heterocycle (N—C═N) of aromatic PCN, which is considered to be the major carbon in the skeleton of the conjugated system [62]. The largest peak of N 1s in Fig. 4d locating at 398.6 eV is corresponded to the sp^2-bonded nitrogen in the form of C—N═C, while the peak at 400.2 eV is caused by the tertiary nitrogen N—$(C)_3$ groups. These two nitrogen together with the sp^2-bonded carbon make up the heptazine heterocyclic ring (C_6N_7) units [61]. All the peaks of C 1s and N 1s are almost the same as those of the pristine carbon nitride [63]. As shown in EDX spectra of **1a**/CNU samples (Fig. S3), there are no peaks belonging to any elements without C, N, Co and O elements. These results are further proved that the **1a** cubanes uniformly distribute in the framework of PCN.

The optical features of the CNU before and after impregnation with the **1a** were analyzed by UV–vis diffuse reflectance (DRS) spectra and room-temperature photoluminescence (PL). In Fig. 5a, the optical absorption band edge enhanced from 450 to 750 nm as the **1a** content increased. However, few differences arising from the inherent band structure of the CNU polymer could be seen after the modification, this is mainly because low amounts of **1a** contents. The enhanced optical absorption in the visible light region is mainly due to the existence of **1a** on the surface of CNU, and the optimization in the electronic structure of the CNU tends to strengthen the charge carrier transfer in the homogeneous system. This can be certified by the following experiments. In the Fig. 5b, all of the samples show similar peaks centered at about 460 nm. The peak intensity decreased as the loading content increased. The pure CNU exhibits strong PL emission signals, which represent serious recombination of the photogenerated electrons and the holes. With the increased of **1a** content, substantial PL quenching was observed, indicative of greatly suppressed radiative electron-hole recombination in **1a**/CNU with respect to CNU. This phenomenon indicates that the recombination rate of the photogenerated charge carrier is enormously restrained. In this case, with the help of **1a**, the migration rate of electron-hole pairs is greatly increased. On the other hand, improved charge separation results in the reduced photoluminescence lifetime of photogenerated holes in the **1a**/CNU (Fig. 5c), indicating that much more holes are transfer to the **1a**, which is benefit the water oxidation reaction. It is can be further revealed by the room-temperature electron paramagnetic resonance (EPR) analysis (Fig. 5d). Obviously, both the pure and modified CNU samples show one single Lorentzian line in the same magnetic field region with a g-value of 2.0034. This signal is attributed to unpaired electron on the carbon atoms of the aromatic rings within π-boned clusters, which is considered as the typical signal of CNU [27,28]. The EPR intensity greatly strengthened when the **1a** modified, indicating that the more electrons are captured by the CNU. Moreover, when the samples were illuminated under light, a significantly enhanced EPR signal was observed. These results revealed that efficient photochemical methods contribute to the generation of radical pairs in modified samples, which is helpful to accelerate the transfer rate of electron-hole pairs.

To further reveal the properties of the developed **1a**/CNU materials, electrochemical experiments were performed. Fig. 6a shows the polarization curves of both pure and **1a**-optimized CNU. The positive current in the range of 1.66–2.14 V *vs.* RHE can be ascribed to O_2 evolution. Evidently, a much reduced over-potential can be found when **1a** was severed as co-catalyst in comparison with pure CNU. This is beneficial for promoting multiple-electron water oxidation kinetics and reducing excessive driving potentials. The charge transfer rate in the dark was also studied by electrochemical impedance spectroscopy (Fig. 6b). Both of the two samples show similar semicircular Nyquist plots. However, a remarkably decreased radius was found when CNU was modified with a certain amount of **1a**, implying that a reduced charge carrier transfer impedance at the sample-solution interface can be obtained, which provides a resistance-less path for fast charge transfer between **1a** and CNU interface. The accelerated charge carrier transfer rate can also be explored by the photoelectrochemical experiments. In Fig. 6c, it shows the current density of modified CNU is about three times higher than that of pure CNU. This suggests the electrical conductivity was improved at the electrode interface, revealing the efficiently reduced over-potential for water oxidation and a better photocatalytic performance can be expected.

In the next set experiments, we studied the photocatalytic activity of a series of cobalt-based co-catalysts complexes modified CNU for water oxidation reaction to liberate O_2 from water. The photocatalytic behaviour of the co-catalysts modified CNU is evaluated in an assay of

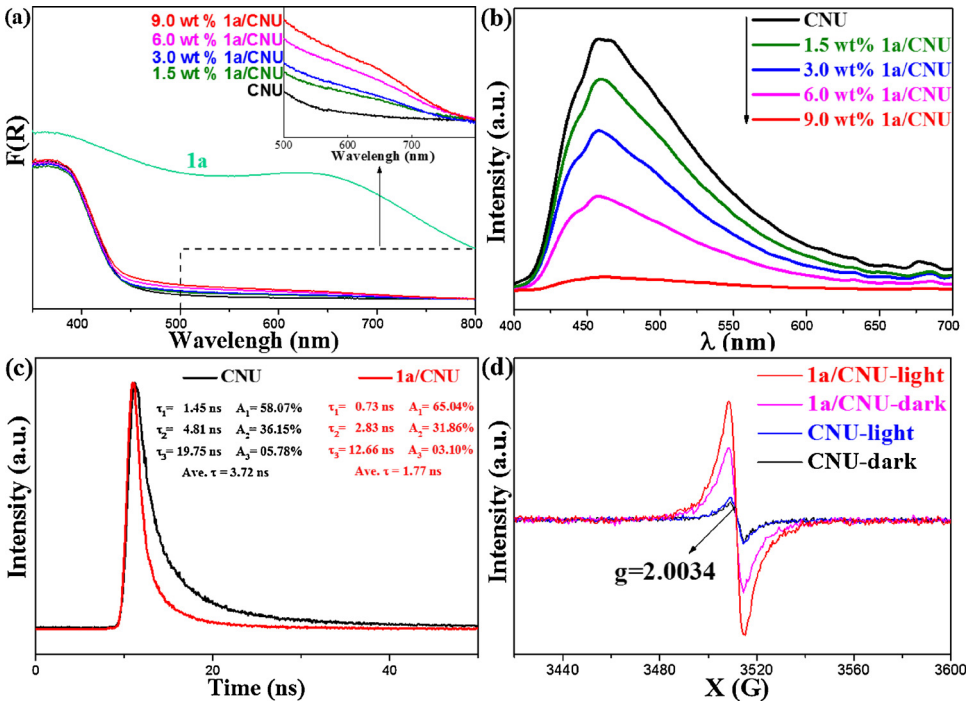

Fig. 5. (a) UV–vis DRS spectra, (b) room-temperature PL spectra, (c) photoluminescence lifetime decay spectra and (d) EPR signals for pure and **1a** modifed CNU samples.

water oxidation in the presence of $AgNO_3$ as electrons trapping agent and thus leaving the holes with sufficient chemical potentials to oxidize water. We firstly checked the activity of different cobalt-based co-catalysts complexes modified CNU. In Fig. 7a, it is clear that the oxygen evolution rate (OER) is dramatically increased after loading Co_4O_4 as an effective molecular co-catalyst than others cobalt-based solid co-catalysts, which demonstrated the advantages of higher activity of water oxidation system modified with molecular co-catalyst. The activity of the OER is expected to be tuned by the different substituent groups on the pyridine, showing an order of **1a** > **1d** > **1c** > **1e** > **1b** (Fig. S4). In Fig. 7b, different content of **1a**-modified CNU for water oxidation reaction are studied. The activity is firstly increased and then decreased. The OER of pure CNU under UV − vis light irradiation (λ ≥ 300 nm) is 1.5 μmol h^{-1}. When the loading content of **1a** is 1.5 wt.%, the OER is dramatically increased to 24 μmol h^{-1}, which is 16 times higher than that of pure CNU. The optimum loading content is determined as 3.0 wt.%, with the best oxygen evolution rate of 29 μmol h^{-1}. This value is 19 times higher than that of pristine CNU. On further increase of loading content to 6.0 wt.% and 9.0 wt.%, the OER is decreased to 24.9 μmol h^{-1} and 16.7 μmol h^{-1}, respectively. This is mainly due to

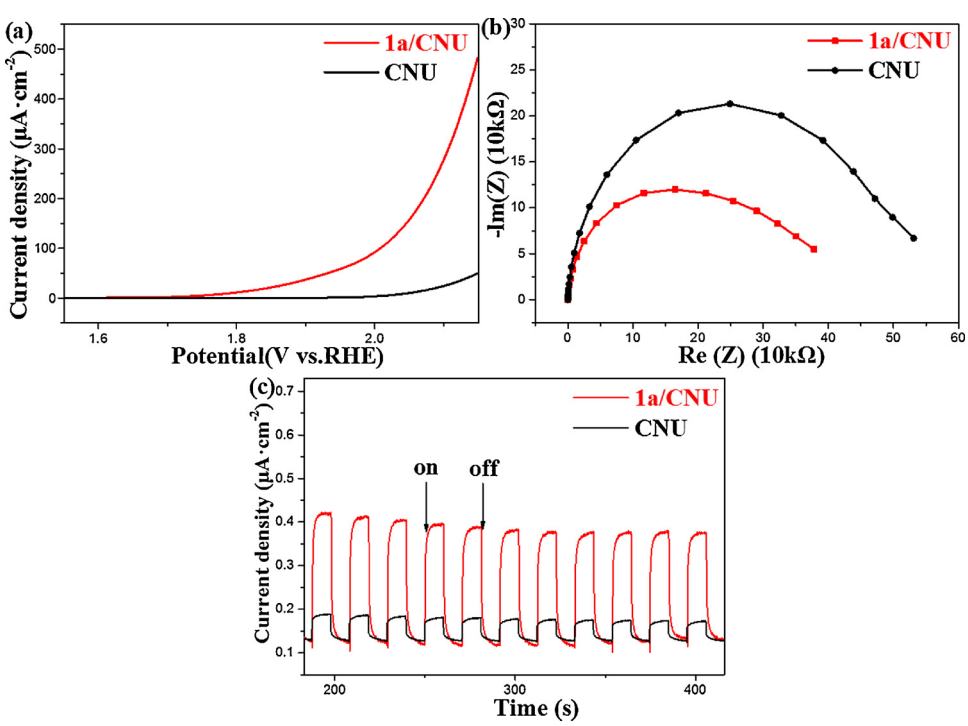

Fig. 6. (a) Polarization curves in the dark of CNU and **1a**/CNU electrodes (*vs.* RHE) in 0.2 M Na_2SO_4 solution, (b) Nyquist plots of electrochemical impedance spectroscopy in the dark of CNU and **1a**/CNU electrodes at 0.4 V (*vs.* RHE) and (c) Transient photocurrent generation from **1a**/CNU/ITO electrodes at −0.2 V (*vs.* RHE) in 0.2 M Na_2SO_4 solution under light irradiation.

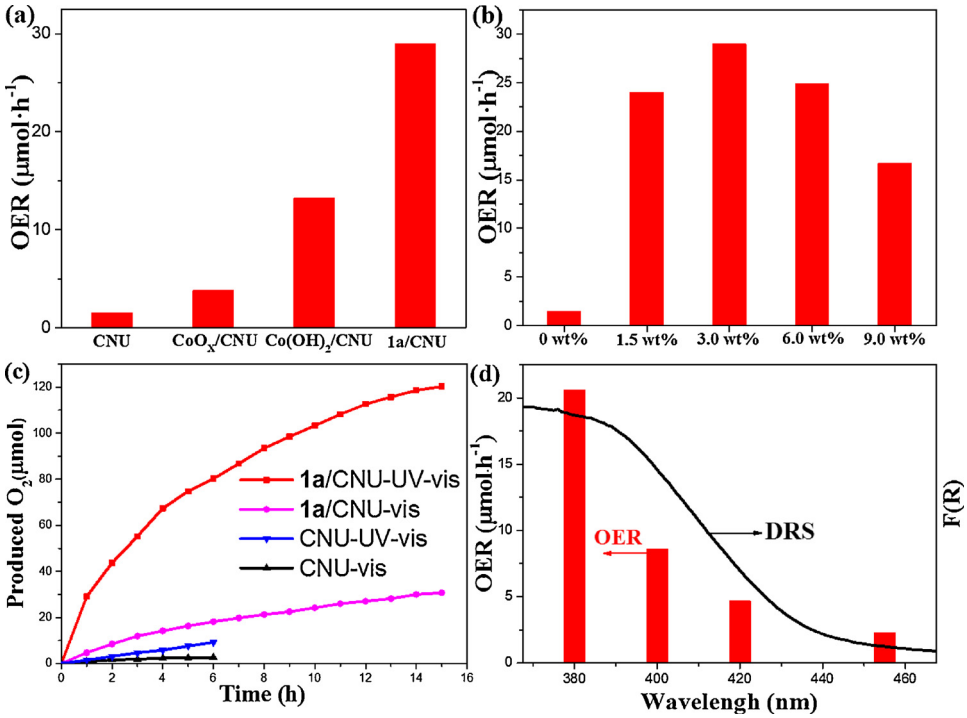

Fig. 7. (a) The activity of water oxidation reaction for different cobalt-based co-catalysts complexes modified CNU and (b) different mass ratio of **1a** loading on the CNU under UV–vis irradiation (λ ≥ 300 nm), (c) a long time performance test of produced O_2 for CNU and **1a**/CNU, and (d) wavelength dependence of the O_2 evolution rate for **1a**/CNU under UV–vis and visible irradiation.

the excessive loading of **1a** that blocks the optical absorption of CNU. The stability of photocatalyst modified by cocatalyst is an important factor worthy of consideration. The long time photocatalytic performance tests of CNU and **1a**/CNU for water oxidation were carried out under both UV–vis and visible light irradiation in Fig. 7c. The amounts of evolved gases reached 120.3 μmol and 30.7 μmol after 15 h of persistent irradiation under the UV–vis and visible light, respectively. The reduced OER is ascribed to the deposition of Ag particles on the surface of CNU (generated from the photoreduction of Ag^+) that leads to the light shading effect and hinders the optical absorption [6–8]. Although the oxygen production performance was reduced, it is still active after prolonged irradiation, indicating that the **1a**/CNU is very stable. To identify the universality of the **1a**, we also test some common catalysts (*e.g.* $BiVO_4$, WO_3) for photocatalytic water oxidation. As shown in Fig. S7, it can be observed that the OER rate for all catalysts have been improved after the **1a** modified. Therefore, we can draw a conclusion the **1a** can be used as an effective and universal co-catalyst for water oxidation reaction. We also have evaluated the OER of the **1a**/CNU sample under different specific wavelength illuminations. As shown in Fig. 7d, the OER of the sample is associated with the DRS absorption spectra. When the illumination wavelengths are λ ≥ 380, 400, 420, and 455 nm, the OER values are 20.6, 8.6, 4.7, and 2.3 μmol h^{-1}, respectively. This indicates that the photocatalytic oxygen evolution reaction is indeed promoted by excitation of carbon nitride polymers with the photons.

The known molecular WOCs are used as a precursor to catalyze the active metal oxides, however, the complete identification of the real catalytic species can be challenged. In consideration of the cobalt ion released from the dissociation of molecular WOC would be the precursor of heterogeneous CoO_x, we provide multiple lines of evidence to support that Co_4O_4 is a real co-catalyst rather than a precursor of cobalt oxide in the following part. First, in Fig. S5a, the ^{1}H NMR spectrum of **1a** exhibited three sets of peaks at 8.20 (m,8 H), 7.71 (m,4 H) and 7.21 (m,8 H) ppm for the ortho, para, and meta ring protons of the equivalent pyridines, while the methyl protons of acetate ligands appear as a sharp singlet at 2.06 (s,12 H) ppm. There are no signals belonging to any impurity. The result shows the presence of only one type of environment for the acetate ligands as well as the four pyridine ligands. This indicates that the cobalt centers are equivalent in the solution phase. Second, we kept the **1a** in the air for four months. After four months of storage, the ^{1}H NMR spectra of the **1a** is similar with four months ago (Fig. S5b), indicating the water solution of **1a** is extremely stable. Third, we do not see any nanoparticles in the TEM of the **1a** modified samples (Fig. S6), which is revealed that the **1a** is uniformly dispersed in the framework of CNU without any cobalt oxides.

4. Conclusion

In summary, we have demonstrated the combination of the PCN with a water-soluble molecular co-catalyst Co_4O_4 towards water oxidation. It is not only increases the contact area between the photocatalyst and the co-catalyst, but also provides much more sufficient active sites for reaction. Enhancing the transfer rate of electron-hole pairs and reducing the over-potential for O—O bond formation, results a significant water oxidation activity. Moreover, this work provides new ideas for the design of new materials by incorporating available molecular materials to extend their functionality to wider applications, including CO_2 reduction, pollution purification and fine chemical synthesis.

Acknowledgements

This work was financially supported by the National Key Technologies R&D Program of China (2018YFA0209301), the National Natural Science Foundation of China (21425309, 21761132002, and 21861130353) and the 111 Project.

Appendix A. Supplementary data

Supplementary material related to this article can be found, in the online version, at doi:https://doi.org/10.1016/j.apcatb.2018.07.056.

References

[1] S. Chu, A. Majumdar, Nature 488 (2012) 294–303.
[2] J.G. Mcalpin, T.A. Stich, W.H. Casey, R.D. Britt, Coord. Chem. Rev. 256 (2012) 2445–2452.

[3] G.P. Gardner, Y.B. Go, D.M. Robinson, P.F. Smith, J. Hadermann, A. Abakumov, M. Greenblatt, G.C. Dismukes, Angew. Chem. Int. Ed. 124 (2012) 1648–1651.
[4] W. Bi, X. Li, Z. Lei, J. Tao, L. Zhang, Q. Zhang, L. Yi, C. Wu, X. Yi, Nat. Commun. 6 (2015) 8647.
[5] M.M. Najafpour, T. Ehrenberg, M. Wiechen, P. Kurz, Angew. Chem. Int. Ed. 49 (2010) 2233–2237.
[6] X. Wang, K. Maeda, A. Thomas, K. Takanabe, G. Xin, J.M. Carlsson, K. Domen, M. Antonietti, Nat. Mater. 8 (2009) 76–80.
[7] K. Maeda, X. Wang, Y. Nishihara, D. Lu, M. Antonietti, K. Domen, J. Phys. Chem. C 113 (2009) 4940–4947.
[8] F. Goettmann, A. Thomas, M. Antonietti, Angew. Chem. Int. Ed. 46 (2007) 2717–2720.
[9] Y. Cui, Z. Ding, X. Fu, X. Wang, Angew. Chem. Int. Ed. 51 (2012) 11814–11818.
[10] P. Yang, R. Wang, M. Zhou, X. Wang, Angew. Chem. Int. Ed. 57 (2018) 8674–8677.
[11] P. Yang, H. Ou, Y. Fang, X. Wang, Angew. Chem. Int. Ed. 56 (2017) 3992–3996.
[12] D. Zheng, C. Pang, X. Wang, Chem. Commun. 51 (2015) 17467–17470.
[13] Z. Lin, X. Wang, Angew. Chem. Int. Ed. 52 (2013) 1735–1738.
[14] G. Zhang, M. Zhang, X. Ye, X. Qiu, S. Lin, X. Wang, Adv. Mater. 26 (2014) 805–809.
[15] K. Maeda, R. Kuriki, M. Zhang, X. Wang, O. Ishitani, J. Mater. Chem. A 2 (2014) 15146–15151.
[16] S. Wang, J. Lin, X. Wang, Phys. Chem. Chem. Phys. 16 (2014) 14656–14660.
[17] Y. Fang, X. Wang, Chem. Commun. 54 (2018) 5674–5687.
[18] Y. Cui, Y. Tang, X. Wang, Mater. Lett. 161 (2015) 197–200.
[19] Y. Cui, Z. Ding, P. Liu, M. Antonietti, X. Fu, X. Wang, Phys. Chem. Chem. Phys. 14 (2012) 1455–1462.
[20] G. Liu, P. Niu, C. Sun, S.C. Smith, Z. Chen, G.Q. Lu, H.M. Cheng, J. Am. Chem. Soc. 132 (2010) 11642–11648.
[21] F. Guo, Y. Hou, A.M. Asiri, X. Wang, Chem. Commun. 53 (2017) 13221–13224.
[22] K. Takanabe, K. Kamata, X. Wang, M. Antonietti, J. Kubota, K. Domen, Phys. Chem. Chem. Phys. 12 (2010) 13020–13025.
[23] Y. Wang, J. Hong, W. Zhang, R. Xu, Catal. Sci. Technol. 3 (2013) 1703–1711.
[24] J. Sun, J. Zhang, M. Zhang, M. Antonietti, X. Fu, X. Wang, Nat. Commun. 3 (2012) 1139.
[25] J. Zhang, F. Guo, X. Wang, Adv. Funct. Mater. 23 (2013) 3008–3014.
[26] Y.S. Jun, E.Z. Lee, X. Wang, W.H. Hong, G.D. Stucky, A. Thomas, Adv. Funct. Mater. 23 (2013) 3661–3667.
[27] J. Zhang, X. Chen, K. Takanabe, K. Maeda, K. Domen, J.D. Epping, X. Fu, M. Antonietti, X. Wang, Angew. Chem. Int. Ed. 49 (2010) 441–444.
[28] J. Zhang, G. Zhang, X. Chen, S. Lin, L. Möhlmann, G. Dołęga, G. Lipner, M. Antonietti, S. Blechert, X. Wang, Angew. Chem. Int. Ed. 51 (2012) 3183–3187.
[29] H. Ou, X. Chen, L. Lin, Y. Fang, X. Wang, Angew. Chem. Int. Ed. 57 (2018) 8729–8733.
[30] Y. Wang, R. Shi, J. Lin, Y. Zhu, Energy Environ. Sci. 4 (2011) 2922–2929.
[31] J. Zhang, M. Zhang, R.-Q. Sun, X. Wang, Angew. Chem. Int. Ed. 51 (2012) 10145–10149.
[32] J. Ran, J. Zhang, J. Yu, M. Jaroniec, S.Z. Qiao, Chem. Soc. Rev. 43 (2014) 7787–7812.
[33] G. Zhang, Z.-A. Lan, X. Wang, Chem. Sci. 8 (2017) 5261–5274.
[34] J. Sato, N. Saito, Y. Yamada, K. Maeda, T. Takata, J.N. Kondo, M. Hara, H. Kobayashi, K. Domen, Y. Inoue, J. Am. Chem. Soc. 127 (2005) 4150–4151.
[35] R. Abe, K. Shinmei, K. Hara, B. Ohtani, Chem. Commun. 24 (2009) 3577–3579.
[36] R. Li, Z. Chen, W. Zhao, F. Zhang, K. Maeda, B. Huang, S. Shen, K. Domen, C. Li, J. Phys. Chem. C 117 (2013) 376–382.
[37] F. Zhang, A. Yamakata, K. Maeda, Y. Moriya, T. Takata, J. Kubota, K. Teshima, S. Oishi, K. Domen, J. Am. Chem. Soc. 134 (2012) 8348–8351.
[38] S.K.M. Su, T. Hisatomi, K. Maeda, Y. Moriya, K. Domen, J. Am. Chem. Soc. 134 (2012) 19993–19996.
[39] K. Kamata, K. Maeda, D. Lu, Y. Kako, K. Domen, Chem. Phys. Lett. 470 (2009) 90–94.
[40] Y. Hou, C. Zheng, Z. Zhu, X. Wang, Chem. Commun. 52 (2016) 6888–6891.
[41] W. Bi, X. Li, L. Zhang, T. Jin, L. Zhang, Q. Zhang, Y. Luo, C. Wu, Y. Xie, Nat. Commun. 6 (2015).
[42] T.M. Mccormick, B.D. Calitree, A. Orchard, N.D. Kraut, F.V. Bright, M.R. Detty, R. Eisenberg, J. Am. Chem. Soc. 132 (2010) 15480–15483.
[43] P. Du, R. Eisenberg, Energy Environ. Sci. 5 (2012) 6012–6021.
[44] Y. Umena, K. Kawakami, J.R. Shen, N. Kamiya, Nature 473 (2011) 55–60.
[45] B. Loll, J. Kern, W. Saenger, A. Zouni, J. Biesiadka, Nature 438 (2005) 1040–1044.
[46] M. Yagi, M. Kaneko, Chem. Rev. 101 (2001) 21–36.
[47] A. Sartorel, M. Bonchio, S. Campagna, F. Scandola, Chem. Soc. Rev. 42 (2013) 2262–2280.
[48] S. Berardi, G.G. La, M. Natali, I. Bazzan, F. Puntoriero, A. Sartorel, F. Scandola, S. Campagna, M. Bonchio, J. Am. Chem. Soc. 134 (2012) 11104–11107.
[49] P.F. Smith, C. Kaplan, J.E. Sheats, D.M. Robinson, N.S. Mccool, N. Mezle, G.C. Dismukes, Inorg. Chem. 53 (2014) 2113–2121.
[50] J.G. Mcalpin, T.A. Stich, C.A. Ohlin, Y. Surendranath, D.G. Nocera, W.H. Casey, R.D. Britt, J. Am. Chem. Soc. 133 (2011) 15444–15452.
[51] N.S. Mccool, D.M. Robinson, J.E. Sheats, G.C. Dismukes, J. Am. Chem. Soc. 133 (2011) 11446–11449.
[52] K. Dimitrou, K. Folting, W.E. Streib, G. Christou, J. Am. Chem. Soc. 115 (1993) 6432–6433.
[53] R. Chakrabarty, S.J. Bora, B.K. Das, Inorg. Chem. 46 (2007) 9450–9462.
[54] G. Mattioli, P. Giannozzi, A. Amore Bonapasta, L. Guidoni, J. Am. Chem. Soc. 135 (2013) 15353–15363.
[55] X. Li, P.E. Siegbahn, J. Am. Chem. Soc. 135 (2013) 13804–13813.
[56] P.F. Smith, L. Hunt, A.B. Laursen, V. Sagar, S. Kaushik, K.U.D. Calvinho, G. Marotta, E. Mosconi, F.D. Angelis, G.C. Dismukes, J. Am. Chem. Soc. 137 (2015) 15460–15468.
[57] Y. Wang, F. Li, H. Li, L. Bai, L. Sun, Chem. Commun. 52 (2016) 3050–3053.
[58] Y. Wang, F. Li, X. Zhou, F. Yu, J. Du, L. Bai, L. Sun, Angew. Chem. Int. Ed. 56 (2017) 6911–6915.
[59] Z. Yu, P.R. Cantwell, Q. Gao, D. Yin, Y. Zhang, N. Zhou, G.S. Rohrer, M. Widom, J. Luo, M.P. Harmer, Science 358 (2017) 97–101.
[60] M. Tabbal, T. Christidis, S. Isber, P. Merel, M.A. El Khakani, M. Chaker, A. Amassian, L. Martinu, J. Appl. Phys. 98 (2005) 044310.
[61] A. Vinu, K. Ariga, T. Mori, T. Nakanishi, S. Hishita, D. Golberg, Y. Bando, Adv. Mater. 17 (2005) 1648–1652.
[62] G. Zhang, J. Zhang, M. Zhang, X. Wang, J. Mater. Chem. 22 (2012) 8083–8091.
[63] J. Zhang, M. Zhang, C. Yang, X. Wang, Adv. Mater. 26 (2014) 4121–4126.